

Calcination - Assisted Hydrothermal Synthesis and Electrochemical Performance of Fe₃O₄/HSFC Nanocomposites as Li-ion Batteries Anodes

Zilin Mo¹, Jianwu Sun¹, Aimiao Qin^{1*}, Shuoping Chen¹, Lei Liao^{2*}, Rui Du¹, Kaiyou Zhang¹

¹ Guangxi Key Laboratory in Universities of Clean Metallurgy and Comprehensive Utilization for Non-ferrous Metals Resources, Key Lab New Processing Technology for Nonferrous Metals & Materials Ministry of Education, College of Materials science & engineering, Guilin University of Technology, Guilin, China

² Guangxi Key Laboratory of Environment Pollution Control Theory and Technology, College of Environmental Science and Engineering, Guilin University of Technology
Guilin, China

*E-mail: 2005032@glut.edu.cn, fangqiu2001@163.com

Received: 20 July 2017 / Accepted: 7 September 2017 / Published: 12 October 2017

Hydrothermal sisal fiber carbon (HSFC) was synthesized by a two-step hydrothermal modification with sisal fiber as raw material. Then Fe₃O₄/HSFC nanocomposites were prepared by combining HSFC with nanostructures of Fe₃O₄ via a hydrothermal process assisted by calcinating. The structure and morphology of Fe₃O₄/HSFC nanocomposites were characterized by powder X-ray diffraction and scanning electron microscopy (SEM), and their electrochemical performances were tested by constant current charge-discharge tests. The first coulomb efficiency of resulted Fe₃O₄/HSFC nanocomposite is 64% at the current density of 50 mA g⁻¹ and the calcination temperature of 600 °C. The reversible capacity can maintain 610 mA h g⁻¹ and 480 mA h g⁻¹ at the current densities of 50 and 500 mA g⁻¹ after 50 cycles, respectively. The results show that modification with Fe₃O₄ nanoparticles is an effective method to improve the electrochemical performances of the HSFC-based materials.

Keywords: sisal fiber carbon; hydrothermal treatment; Fe₃O₄ nanoparticles; calcination; electrochemical performance

1. INTRODUCTION

Biomass carbon is expected to become a new type anode material for lithium-ion batteries (LIBs) due to its low cost, abundant reserves, pollution-free and high capacity, which may replace commercialized graphite carbon materials [1-2]. In many biomass raw materials, sisal fiber

extracted from the leaf of sisal plant, has been proved to be a good precursor for preparing high-quality biomass carbon, due to its porous structure and high relative strength [3-5]. In our previous investigation, hydrothermal sisal fiber carbon(HSFC) was synthesized and showed a good reversible capacity of 728 mA h g^{-1} in the first discharge, which much higher than the theoretical specific capacity of graphite carbon (372 mA h g^{-1}), which can be potential anode of LIBs. However, its relative low first coulomb efficiency (about 52%) and reversible capacity at the stable stage (305 mAhg^{-1} after 50 cycles) still fail to meet the need for commercial applications [6]. The reason is probably that, compared with stable commercial graphite structure, the structures of biomass carbons(such as HSFC) are easy to collapse[7-11]. Thus, it is still a great challenge for HSFC to be a good anode material with high coulomb efficiency and reversible capacity at high current densities.

It has been proved that, the modification of carbon materials by using transition metal compounds can improve their conductivity, reversible capacity and cycle capacity [12-13]. Among many transition metal anode materials, iron oxides have received a lot of interest due to their advantages of high theoretical capacity (up to $800\sim 1000 \text{ mA h g}^{-1}$), low cost, facile preparation and environment-friendly [14-15]. Thus, the combination of carbon and iron oxide can compensate the poor conductivity of iron oxide and inhibit the volume expansion of iron oxide in the electrochemical reaction process. On the other hand, iron oxide can relieve the mechanical fatigue of the carbon material caused by Li^+ embedding and stripping in the charging and discharging process, and significantly increases the reversible capacity of the carbon material. For example, He et al reported the synthesis of CNTs/ Fe_3O_4 nanocomposites by coprecipitation method with $(\text{NH}_4)_2\text{Fe}(\text{SO}_4)_2 \cdot 6\text{H}_2\text{O}$ and $\text{NH}_4\text{Fe}(\text{SO}_4)_2 \cdot 12\text{H}_2\text{O}$ as raw materials, The initial discharge and charge capacity of the CNTs– $66.7 \text{ wt.}\% \text{ Fe}_3\text{O}_4$ nanocomposite electrode are 988 mAh g^{-1} and 661 mAh g^{-1} , respectively. The recharge capacity retention after 145 cycles remains 645 mAh g^{-1} , which is significantly higher than that of the commercial graphite material[16]. Han et al prepared $\text{FeO}_x/\text{carbon}/\text{graphite}$ composites in one step by using the solution combustion synthesis method, the $\text{FeO}_x/\text{carbon}/\text{graphene}$ ($31.4 \text{ wt.}\% \text{ graphene}$) delivered a higher discharge capacity of 824 mAh g^{-1} after 100 cycles at 0.4 A g^{-1} , in comparison to the value of 301 mAh g^{-1} for the composite without graphene[17]. Chang et al. successfully connected Fe_3O_4 nanospheres with rGO flakes to form rGO- Fe_3O_4 composites using the simple and effective hydrothermal method, which exhibited a stable reversible capacity of 668 mAh g^{-1} up to 200 cycles by comparison of the results with those from bare Fe_3O_4 nanospheres(capacity declined to 117 mAh g^{-1} only at the 200th cycle)[18].

It can be expected that, modified HSFC with iron oxide nanostructures can be a good strategy to obtain better anode materials for LIB. In our recent investigation, nano iron oxide/SFCs composites were fabricated by hydrothermal method, the composites consisted of $\alpha\text{-Fe}_2\text{O}_3$ and $\alpha\text{-FeOOH}$ mixture phase prepared at 120°C delivered a reversible capacity of 359 mA h g^{-1} at a current density of 50 mA g^{-1} after 40 cycles[19]. Subsequently, nanostructures of $\text{Fe}_2\text{O}_3/\text{SFC}$ composites were successfully synthesized, which showed a better electrochemical performances with a first coulomb efficiency of 61.5% and a reversible capacity of 500 mAhg^{-1} after 50 cycles[20].

Hydrothermal reaction is a simple and efficient approach to synthesis of transition metal related compounds[21]. In this work, in order to further explore the modification of HSFC-based materials, using HSFC, urea and iron trichloride ($\text{FeCl}_3 \cdot 6\text{H}_2\text{O}$) as raw materials, nanostructures of

Fe₃O₄/HSFC composites were successfully prepared via hydrothermal reaction. The effects of calcination temperature and raw material ratio on the morphology of Fe₃O₄/HSFC nanocomposites were investigated. The Fe₃O₄/HSFC nanocomposites display good electrochemical performances, which can be a potential anode material of LIB.

2. EXPERIMENTAL

2.1 Synthesis of Fe₃O₄/HSFC nanocomposites

Fig. 1 shows a schematic illustration of the synthesis procedure of Fe₃O₄/HSFC nanocomposites, which includes two main steps, the synthesis of HSFC matrix and Fe₃O₄/HSFC nanocomposites.

Synthesis of HSFC: The sisal fibers (SFs) were purchased from Guangxi Sisal Group Co., Ltd. The maize-yellow SFs were washed with deionized water to remove the impurities, cut into small pieces (~2cm in length) and dried in the oven at 80°C.

And then the SFs were treated by a two-step hydrothermal reaction. A mixture of 2.0g SFs and 75mL 1M hydrochloric acid (HCl) was placed in a 100 mL Teflon-lined stainless steel autoclave. The mixture solution was heated at 160°C for 12 h, and then cooled to room temperature. The tawny prepared materials were collected and washed by deionized water until the pH dropped to 7, dried in the oven at 80°C, and placed in another 100 mL Teflon-lined stainless steel autoclave. The hydrazine hydrate (75 mL) was added into the autoclave, and then heated at 120°C for 12 h. The reaction product was washed with deionized water to neutral again, and then put into a nickel crucible, calcined in a tube furnace at 700°C for 0.5 h under nitrogen atmosphere (the heating rate kept at 3°C min⁻¹). After that, the carbonaceous product was cooled down to room temperature naturally, collected, and ground fully (~200 meshes) in an agate mortar. The obtained product is denoted as HSFC.

Preparation of Fe₃O₄/HSFC nanocomposites: The Fe₃O₄/HSFC nanocomposites were synthesized by a hydrothermal method. According to the raw material formulation (shown in Table 1), FeCl₃·6H₂O, CO(NH₂)₂ and HSFC were mixed in a 100 mL Teflon-lined stainless steel autoclave. 75 mL of deionized water was added and stirred with a magnetic stirrer for 0.5 h. And then, the autoclave was sealed and heated at 130°C for 12 h. The reaction mixture was cooled to room temperature, washed by deionized water, dried in an oven at 80°C for 12 h to afford Fe₂O₃/HSFC nanocomposites. The resulted Fe₂O₃/HSFC nanocomposites were placed in a tube furnace and calcined under nitrogen atmosphere with a heating rate of 3°C/min. The calcination temperatures were set as 500°C, 600°C, 650°C, 700°C, respectively, and the calcination time was 0.5 h. After calcination, black powders of Fe₃O₄/HSFC nanocomposites were obtained.

Table 1. The raw material formulation for preparing Fe₃O₄/HSFC nanocomposites.

Sample	FeCl ₃ ·6H ₂ O(g)	CO(NH ₂) ₂ (g)	HSFC (g)	Content of Fe ₃ O ₄ (%)
C-1	0.85	0.3	0.75	25
C-2	1.7	0.6	0.50	49
C-3	2.55	0.9	0.25	74

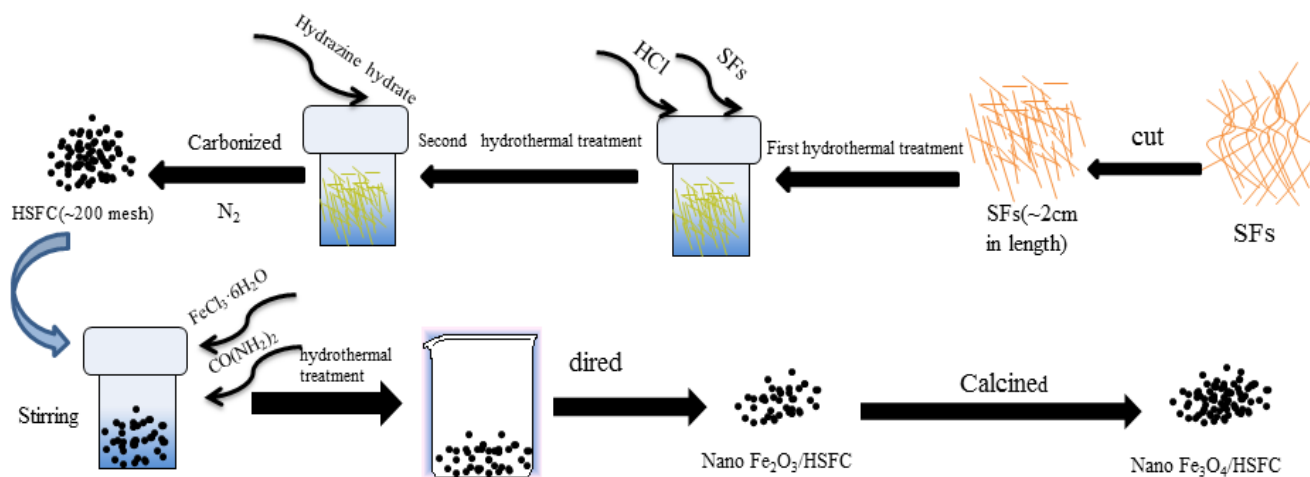


Figure 1. Schematic illustration of the synthesis procedure of Fe₃O₄/HSFC nanocomposites

2.2 Characterization

The surface morphology and composition of the samples were observed by scanning electron microscopy (SEM, S-4800, Hitachi High-Technologies Co.), operated at 5 KV. The crystal structures of the Fe₃O₄/HSFC composites were characterized by powder X-ray diffraction (XRD, X'Pert PRO, PANalytical B.V.), using Cu K α ($\lambda=1.54056\text{\AA}$) as radiation source in the 2θ range of 10~80°.

2.3 Electrochemical measurement

To evaluate the electrochemical performance, coin-type half-cells were assembled using the as-prepared samples as anode materials for lithium-ion batteries. The working electrodes were prepared by mixing the as-synthesized Fe₃O₄/HSFC nanocomposites, conductive carbon black, and poly(vinylbenzene fluoride) binder dispersed in a N-methyl-2-pyrrolidone solution at a weight ratio of 80:10:10, respectively. The as-prepared active material slurry was uniformly spread onto Cu foil and dried in a vacuum oven at 110°C for 12h prior to coin cell assembly. The electrochemical experiments were performed using LIR2025-type coin cells, which were assembled in an argon-filled dry glove box (Super 1220/750, Mikrouna) with Fe₃O₄/HSFC nanocomposites as the working electrode, pure lithium foil as the counter and reference electrodes, polypropylene membrane film as the separator, and 1M LiPF₆ in ethylene carbonate (EC)-dimethyl carbonate (DMC) as electrolyte. Galvanostatic charging-discharging (GCD) measurements were carried out under different current densities in the voltage range between 0.01V and 3.0V on a Neware GCD system. Cyclic voltammetry (CV) was conducted on an electrochemical analyzer (CHI-760D) in the voltage range of 0.01~3.0V (vs. Li⁺/Li) at a scan rate of 0.2mVs⁻¹. Electrochemical impedance spectroscopy (EIS) was tested on the CHI-760D in the frequency range of 0.01~10 KHz. All electrochemical measurements were performed at room temperature.

3. RESULTS AND DISCUSSION

3.1 Structure and Morphology

The crystallographic structure and phase purity of $\text{Fe}_3\text{O}_4/\text{HSFC}$ nanocomposites calcined at 500°C , 600°C , 650°C , 700°C , respectively were examined by XRD. As shown in Fig. 2, The weak, broad diffraction peak at around 24° can be attributed to (002) plane of HSFC, which belongs to the amorphous carbon with noncrystalline structures[6]. Additionally, the peaks at 18.31° , 30.11° , 35.46° , 43.10° , 53.47° , 57.00° , 62.60° , and 74.05° correspond to (111), (220), (311), (400), (422), (511), (440), and (533) lattice planes of molybdenite (JCPDS no.89-0691; space group $\text{Fd}\bar{3}\text{m}$; $a=8.387\text{ \AA}$), which was close to the reported data[22]. It is also implied that the as-prepared composites were successfully converted to Fe_3O_4 during the calcination treatment. Compared with those at other calcination temperatures, the $\text{Fe}_3\text{O}_4/\text{HSFC}$ nanocomposites calcined at 550°C displays slightly weaker diffraction peak intensity, which indicates that relatively low calcination temperature may result in low crystalline Fe_3O_4 in the composites. Meanwhile, it can be observed that the Fe_3O_4 diffraction peaks become narrower and higher with calcination temperature increasing, which indicates that the crystallinity increases and the grains become bigger at the higher temperatures.

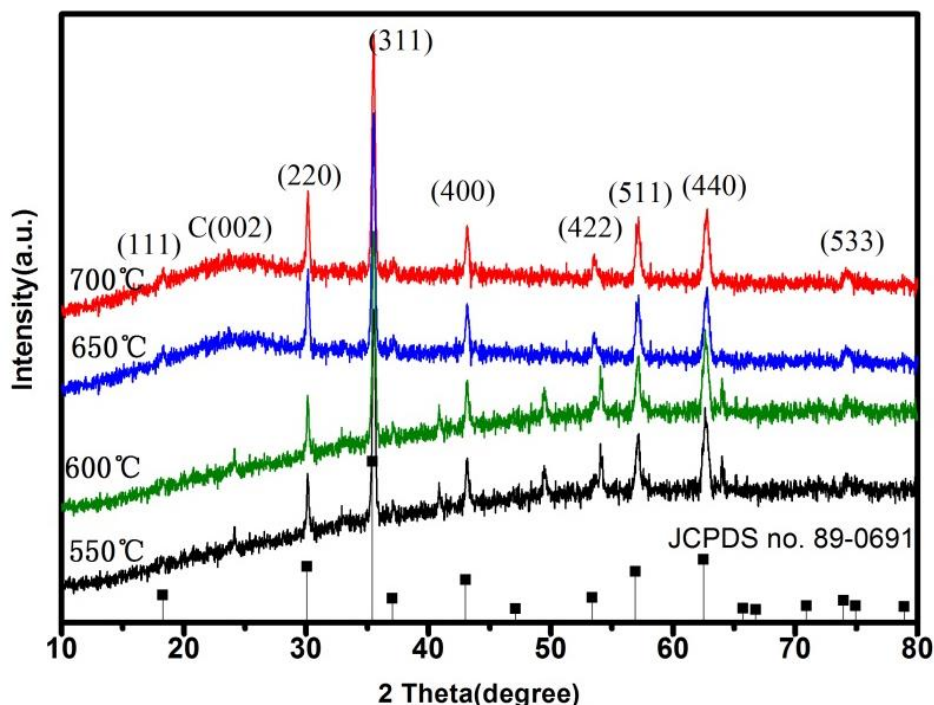


Figure 2. XRD patterns of $\text{Fe}_3\text{O}_4/\text{HSFC}$ nanocomposites calcined at different temperatures.

The SEM images of $\text{Fe}_3\text{O}_4/\text{HSFC}$ nanocomposites calcined at different temperatures are shown in Fig. 3. The sample calcined at 600°C shows a homogeneous morphology, in which the HSFC is uniformly coated with Fe_3O_4 nanoparticles with a size of ca. 100 nm (See Fig. 3b). Lower calcination

temperature (550°C) can result in an incomplete coating of Fe₃O₄ particles to HSFC (See Fig. 3a) . At higher calcination temperature (650°C and 700°C), obvious agglomeration of Fe₃O₄ particles is discovered, forming congeries with much larger particle sizes (See Fig. 3c-3d). The results show that the calcination temperatures have a great influence on the morphology and particle dispersity of the Fe₃O₄/HSFC nanocomposites. The reason is due to the thermal stress concentration at local region in nanocomposites during the heat treatment process[22].

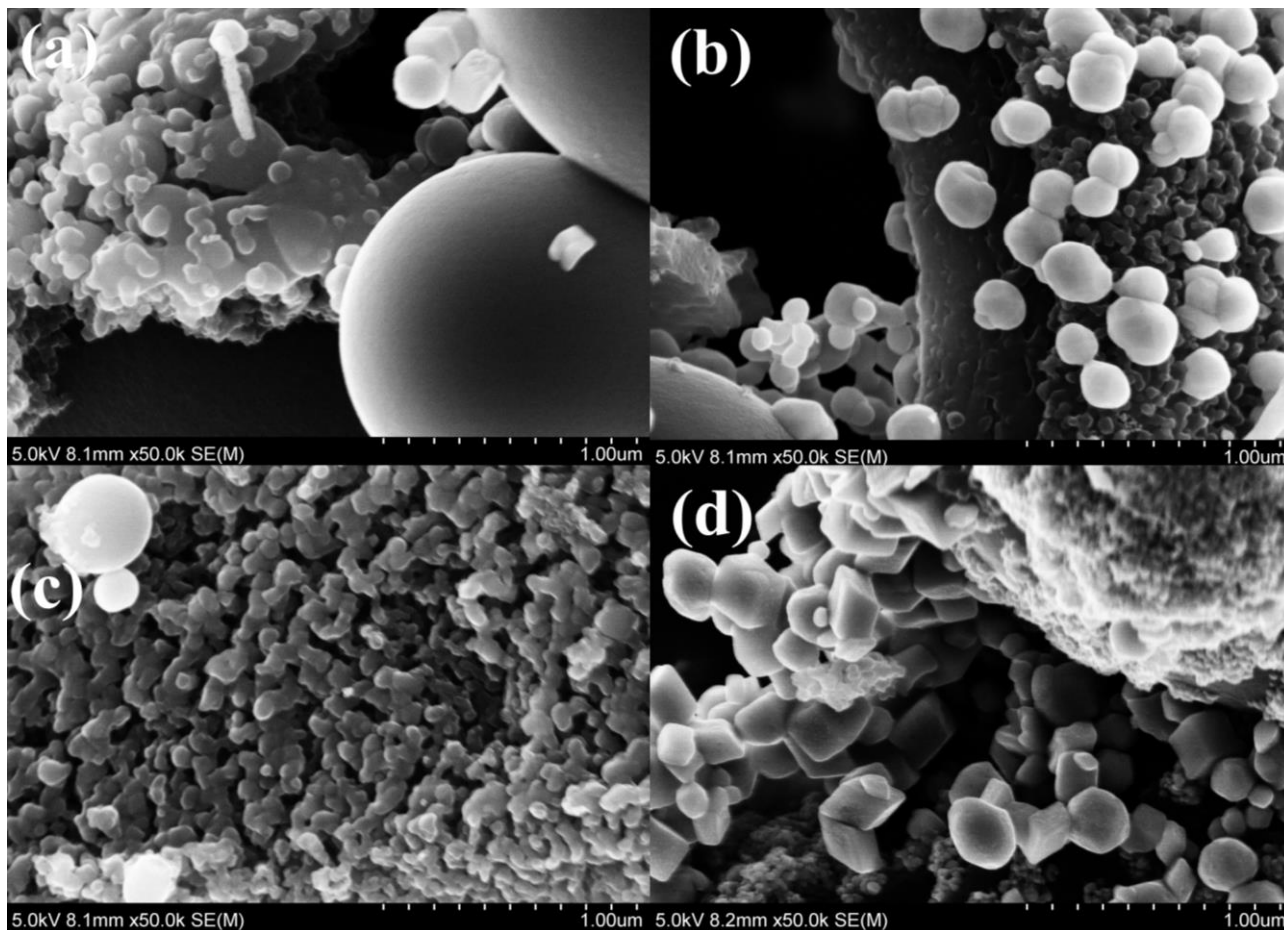


Figure 3. SEM images of Fe₃O₄/HSFC nanocomposites calcined at: (a) 550°C; (b) 600°C; (c) 650°C and (d) 700°C.

The effects of different Fe₃O₄ content on the morphology of Fe₃O₄/HSFC nanocomposites were also investigated. Fig. 4(a-c) shows the SEM images of Fe₃O₄/HSFC nanocomposites containing different weight ratio of Fe₃O₄ which are illustrated in Tab. 1 (C-1, C-2, C-3, which corresponds to the content of Fe₃O₄ as 25%, 49%, 74%, respectively). With the increase of the proportion of FeCl₃·6H₂O in raw material formulation, the particle sizes of Fe₃O₄ particles significantly increase, and the morphology of Fe₃O₄ change from small, dispersed particles to large congeries. Obvious agglomeration of Fe₃O₄ particles is observed in the SEM image of C-3 sample(seen in Fig. 4c).

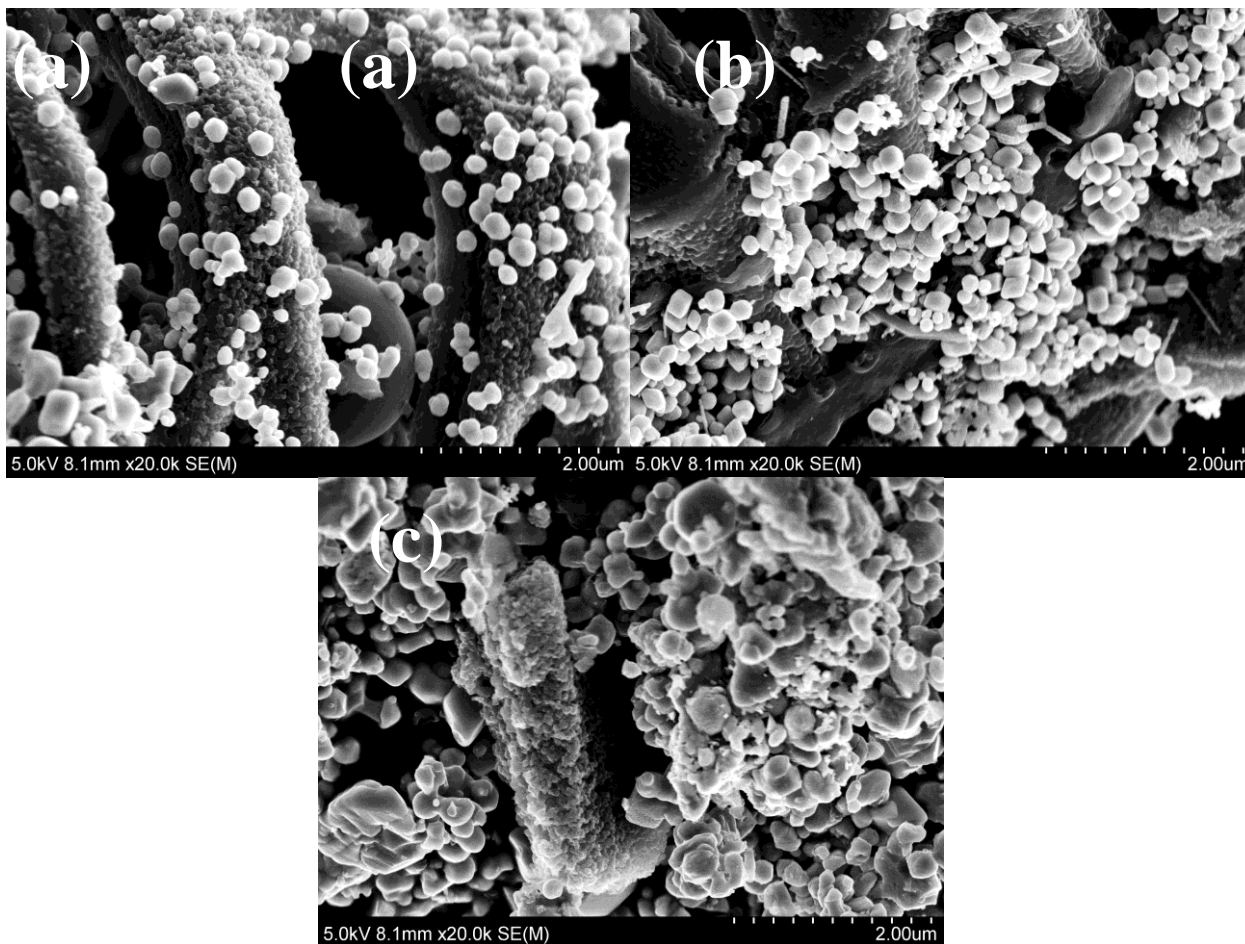


Figure 4. SEM images of $\text{Fe}_3\text{O}_4/\text{HSFC}$ nanocomposites with different Fe_3O_4 content (a) C-1 (25% Fe_3O_4); (b) C-2 (49% Fe_3O_4); (c) C-3 (74% Fe_3O_4).

3.2 Electrochemical properties

To identify electrochemical behavior of the $\text{Fe}_3\text{O}_4/\text{HSFC}$ nanocomposites, cyclic voltammetry (CV) of the half-cell was performed in the range from 0.01 to 3.0 V at a scanning rate of 0.2 mV s^{-1} (seen in Fig. 5). Being similar to the literature[23-27], the first reduction peak appears at around 0.266V, which may be due to the transformation of Fe^{3+} and Fe^{2+} to elemental Fe^0 [23,27]. Compared with the second and third cyclic voltammetry curves, an irreversible electrochemical reaction occurs in the first discharge process, which increases the irreversible capacity, the reason is due to the formation of a solid electrolyte inter phase (SEI) layer that is related to the reaction of electrolyte and electrode material during the first charge/discharge process. In the second and third cyclic voltammetry curves, the reduction peak at around 0.50 V, which can be due to the conversion of Fe^{3+} to Fe^0 [24-25]. In addition, an oxidation peak is observed at about 1.85V for the first time, corresponding to the oxidization of Fe^0 to Fe^{3+} and Fe^{2+} . It is suggested that, structural reorganization and new phase formation of iron oxide are occurred in the first cycle, which results in the shift of first oxidation peak and reduction peak compared with the corresponding peaks in the subsequent cycles.

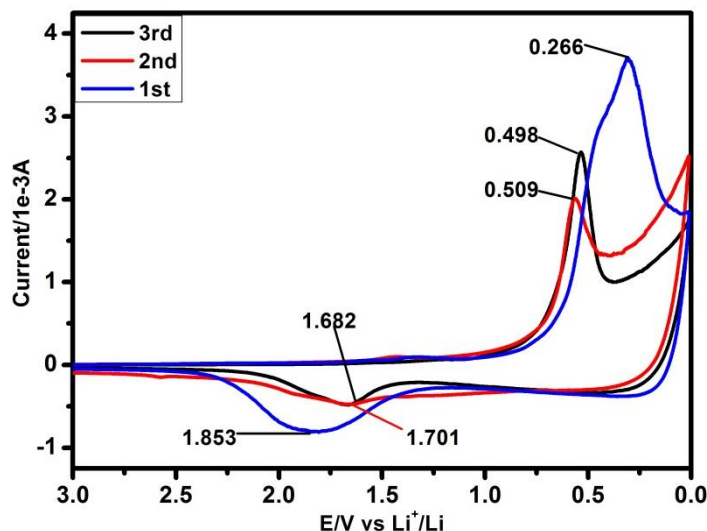


Figure 5. CV curves of $\text{Fe}_3\text{O}_4/\text{HSFC}$ nanocomposites calcined at 600°C

Fig. 6a shows the cycle performance curves of $\text{Fe}_3\text{O}_4/\text{HSFC}$ nanocomposites calcined at different temperatures at a current density of 50mA g^{-1} . The composites calcined at 550°C and 600°C display a good reversible capacity (nearly 1200 mA h g^{-1}) in the first discharge, The composites calcined at 600°C can maintain a good reversible capacity of 605 mA h g^{-1} after 50 cycles, and show a first coulomb efficiency of 64%, which is higher than those of the $\text{Fe}_2\text{O}_3/\text{MSFC}$ nanocomposites (the initial discharge is 1020 mA h g^{-1} , the stable reversible capacity is 500 mA h g^{-1} after 50 cycles, the Coulombic efficiency is 61.5%)[19], which is also great higher than theoretical capacity of Fe_3O_4 (928 mA h g^{-1}) and the commercial graphite (372 mA h g^{-1}). However, the reversible capacity of composites calcined at 550°C decreases dramatically with the cycle number increase, which is only 380 mA h g^{-1} after 50 cycles. The reason is probably that, the structure of composites calcined at 550°C showed a relatively low crystallinity, which tends to be destroyed and results in the decrease of specific capacity. On the other hand, the stability specific capacity of the composites calcined at 650°C and 700°C after 50 cycles is 480 mA h g^{-1} and 465 mA h g^{-1} , respectively, which is lower than that of the composites calcined at 600°C . It is suggested that, the increase of calcination temperatures may lead to the decrease of the interfacial force between the phases, resulting in the large-scale agglomeration and obstructing the insertion and extraction of lithium ions.

Fig. 6b shows the cycling performance of $\text{Fe}_3\text{O}_4/\text{HSFC}$ nanocomposites at a higher current density of 500 mA g^{-1} . The composites calcined at 600°C still display the best cycling performance among the four calcination temperatures. They show a first specific capacity of 1053 mA h g^{-1} , and a stable reversible capacity of 465 mA h g^{-1} after 50 cycles, which is much higher than many previously reported values, such as pure HSFC (305 mA h g^{-1})[28], activated sisal carbons[6], nano iron oxide/SFCs composites[19], and Fe_3O_4 -carbon composite[29]. The remarkable lithium storage properties of $\text{Fe}_3\text{O}_4/\text{HSFC}$ composite are likely related to the synergetic effect of the Fe_3O_4 nanostructures and the HSFC composition. The results prove that the combination of Fe_3O_4 nanoparticles is an effective method to improve the electrochemical performance of HSFC, especially in multiple cycling performance tests at high current density.

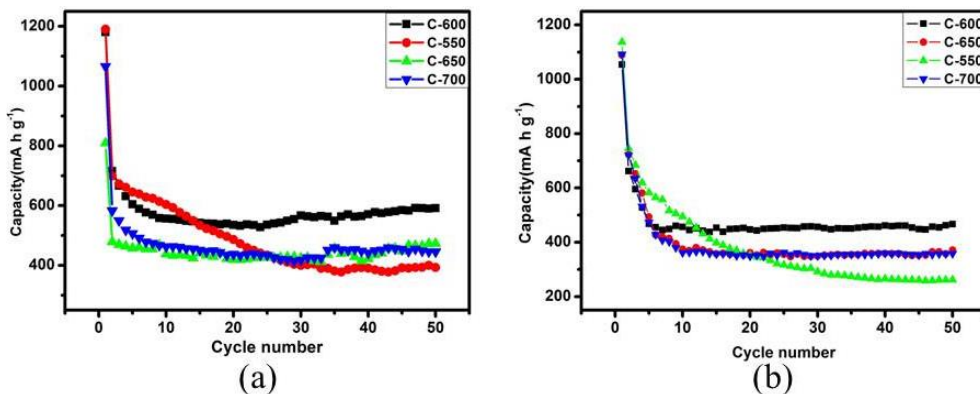


Figure 6. Cycling performances of Fe₃O₄/HSFC nanocomposites prepared at different calcination temperature. Current density: (a)50mA g^{-1} ; (b) 500mA/ g^{-1} .

Fig. 7a shows the Nyquist plots of the Fe₃O₄/HSFC nanocomposites calcined at four different temperatures, and Fig. 7b is the simplified equivalent circuit that was used to interpret the measured results. As shown in Fig. 7a, the slope of the four samples in the low frequency region is similar, indicating that the Fe₃O₄/HSFC nanocomposites calcined at different temperatures have similar diffusion resistance. In the high frequency region, the Fe₃O₄/HSFC nanocomposites calcined at 550 °C have the largest charge transfer resistance (R_{ct}), indicating a weak electronic conductivity, which may be due to that relatively low calcination temperature can result in low crystallinity structure and blocking the lithium ion transfer process[30].

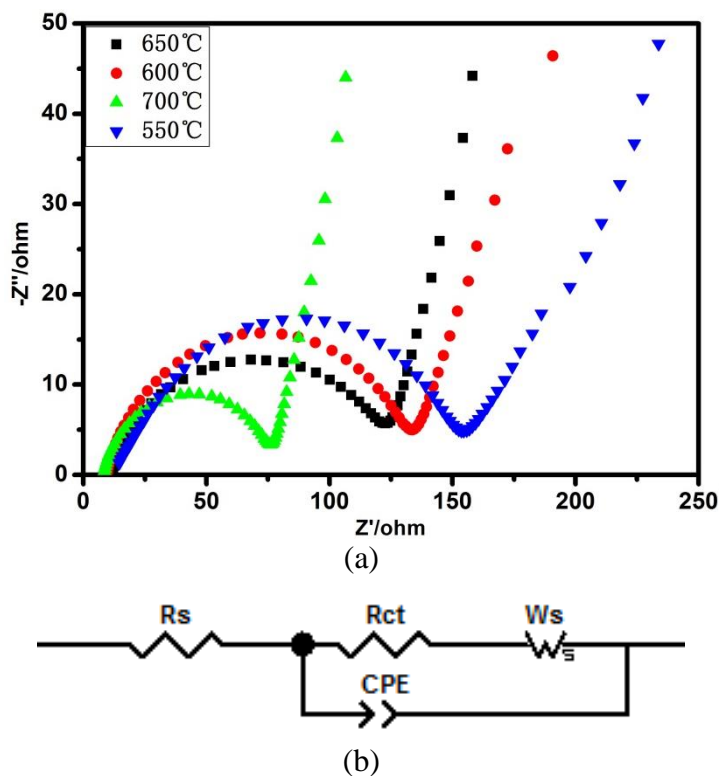


Figure 7. (a) Nyquist plots of the Fe₃O₄/HSFC nanocomposites at different calcination temperatures. (b)Equivalent circuit model

The composites calcined at 600°C-700°C have a smaller charge transfer resistance, at the same time, the samples have a better crystallinity. By comparison, we can see that the calcination temperature has a great impact on the impedance.

Fig. 8a shows the cycle performance of Fe₃O₄/HSFC nanocomposites with different content Fe₃O₄ (C-1, C-2, C-3) at the current density of 50mA g⁻¹. With the increase of the proportion of FeCl₃·6H₂O in raw material formulation, the first specific capacity will escalate, while the stable reversible capacity decreases dramatically after multiple cycles. For example, the C-1 sample shows a reversible capacity of 1260 mA h g⁻¹ at the first discharge, and maintains a reversible capacity of 610 mA h g⁻¹ after 50 cycles, a similar result was observed by the sulfur sisal fiber carbons composites (the initial discharge specific capacity is 1223 mA h g⁻¹), but it only can maintain 400 mA h g⁻¹ after 30 cycles[27]. By contrast, the C-3 sample shows a higher capacity at the first discharge(1380 mA h g⁻¹), but its reversible capacity retains only 420 mA h g⁻¹ after 50 cycles. Under high current density of 500 mA g⁻¹ (Seen in Fig. 8b), the C-1 sample still shows the best electrochemical performances, with a reversible capacity of 1030 mA h g⁻¹ at the first discharge and 482 mA h g⁻¹ after 50 cycles. It is suggested that, suitably introducing Fe₃O₄ nanoparticles is an effective way to improve the electrochemical properties of HSFC-based materials, but the proportion of FeCl₃·6H₂O in raw material formulation should be controlled.

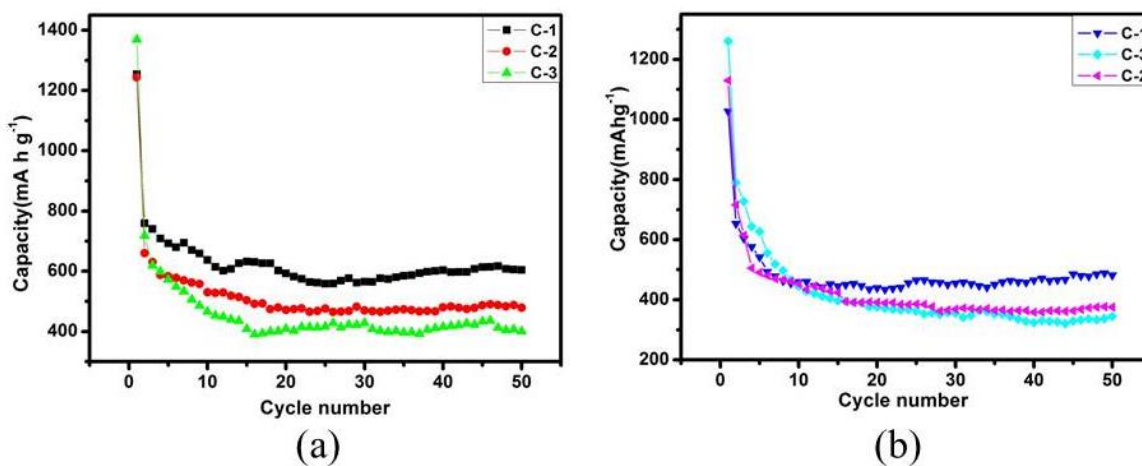


Figure 8. Cycling performances of Fe₃O₄/HSFC nanocomposites with different content of Fe₃O₄ (C-1, C-2, C-3). Current density: (a) 50 mA g⁻¹; (b) 500 mA g⁻¹.

Fig. 9 shows the Nyquist plots of Fe₃O₄/HSFC nanocomposites prepared at various ratios of raw materials. With the increase of the proportion of FeCl₃·6H₂O in raw material formulation, the R_{ct} of the composites gradually increases, mainly due to the poor conductivity of iron oxide[31,32]. The C-1 sample (with the fewest Fe₃O₄ combination) has the smallest R_{ct}, indicating that its structure has a better electrical conductivity and is favourable to the lithium ions insertion and extraction.

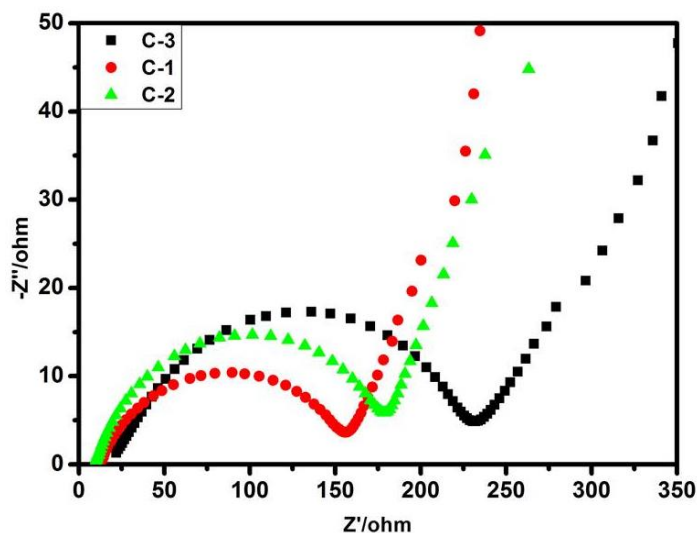


Figure 9. Nyquist plots of $\text{Fe}_3\text{O}_4/\text{HSFC}$ nanocomposites at various content of Fe_3O_4 .

5. CONCLUSIONS

In summary, nanostructures of $\text{Fe}_3\text{O}_4/\text{HSFC}$ composites have been successfully prepared with the hydrothermal method. The morphological and electrochemical properties of the composites are investigated. The results show that the samples calcined at 600°C and introducing appropriate amount of Fe_3O_4 nanoparticles can afford a novel nanocomposites with good electrochemical performances, which is better than that of HSFC and $\text{Fe}_2\text{O}_3/\text{HSFC}$ nanocomposites reported previously, which can provide a significant strategy for the modification of commercial lithium ion anode materials and novel biomass carbon based materials.

ACKNOWLEDGEMENTS

This work is supported by the National Natural Science Foundation of China (No.51564009, 51468011), the Natural Science Foundation of Guangxi (2015GXNSFDA139035), and the Research Funds of Guangxi Experiment Center of Information Science (No. KF1407).

References

1. F. Zhang, K. X. Wang, G. D. Li, J. S. Chen, *Electrochemistry Communications* 11(2009)130.
2. Z. W. Yang, H. G. Guo, X. H. Li, Z. X. Wang, Z. L. Yan, Y. S. Wang, *Journal of Power Sources* 329(2016)339.
3. Y. Li, Y. W. Mai, L. Ye, *Composites Science and Technology* 60(2000)2037.
4. C. S. Wu, *J. Applied Polymer Science* 123(2011) 47.
5. T. P. Mohan, K. Kanny, *Composites: Part A* 43(2012)1989.
6. X. L. Yu, K.Y. Zhang, N. Tian, A.M. Qin, L. Liao, R. Du, C. Wei, *Materials Letters* 142(2015)193.
7. M. Y. Yu, D. L. Cui, L. Kai, Y.S. Yin, Q.L. Wang, C. Lei, *Materials Science and Engineering:B* 121(2005)166.
8. X. M. Lou, J. L. Huang, T. P. Li, H. X. Hu, B. N. Hu, Y. X. Zhang, *Journal of Materials Science:*

- Materials in Electronics* 25(2014)1193.
9. Y. Li, W.V. Roy, L. Lagae, P.M. Vereecken, *Electrochimica Acta* 231(2017)200.
 10. T. Wolfgang, B. J. P. Correa. S. Michael, A. Antonio. G. Michael, *Advanced Energy Materials* 6(2016)1600396.
 11. H. Kim, H. Kim, H. Kim, J. Kim, G. Yoon, K. Lim, W.S. Yoon, K. Kang, *Advanced Functional Materials* 26(2016)5042.
 12. S. Hokkanen, A. Bhatnagar, M. Sillanpää, *Water Research* 91(2016)156.
 13. Z.F. Ma, T.B. Zhao, *Electrochimica Acta* 201(2016)165.
 14. J.S. Cho, Y.J. Hong, Y.C. Kang, *ACS Nano* 9(2015)4026.
 15. Y. Xu, J.D. Feng, X.C. Chen, K. Kierzekd, W. Liu, T. Tang, E. Mijowska, *Rsc Advances* 5(2015)28864.
 16. Y. He, L. Huang, J.S. Cai, X.M. Zheng, S.G. Sun, *Electrochim. Acta* 55(2010)1140.
 17. C.G. Han, C.Y. Zhu, N. Sheng, Y. Aoki, H. Habazaki, T. Akiyama, *Electrochimica Acta* 235(2017)88.
 18. Y. Chang, J. Li, B. Wang, H. Luo, L. Zhi, *Journal of Materials Science & Technology* 30(2014)759.
 19. R. Du, Z. F. Tong, C. Wei, A. M. Qin, K. Y. Zhang, L. Liao. *International Journal of Electrochemical Science* 11(2016) 581.
 20. J. W. Sun, Y. Z. Liu, K. Y. Zhang, Y. F. Wu, A. M. Qin, *Materials Protection* 44(2016)27.
 21. W.Z. Lu, M.Z. Xue, X.L. Chen, C. Chen, *International Journal of Electrochemical Science* 12(2017)1118.
 22. Q. Yu, H. L. Chen, P. Chen, Q. Wang, C. Lu, C. X. Jia, *Journal of Materials Science: Materials in Electronics*, 28(2017)2769.
 23. S. L. Jin, H. G. Deng, D. H. Long, X. J. Liu, L. Zhan, X. Y. Liang, W. M. Qiao, L. C. Ling, *Journal of Power Sources* 196(2011)3887.
 24. G. Y. Zheng, C. Wang, A. Pei, J. Lopez, F. F. Shi, Z. Chen, A. D. Sendek, H. W. Lee, Z. D. Lu, H. Schneider, M. M. Safont-Sempere, S. Chu, Z. N. Bao, Y. Cui, *Acs Energy Letters* 1(2016)1247.
 25. W. X. Wang, S. H. Yang, *Journal of Alloys and Compounds* 695(2016)3249.
 26. J. S. Chen, Y. M. Zhang, X. W. Lou. *Acs Applied Materials & Interfaces*. 3(2011)3276.
 27. M. Z. Zou, L. L. Wang, J. X. Li, L. H. Guan, Z. G. Huang, *Electrochimica Acta*, 233(2017)85.
 28. R. Du, Z. F. Tong, C. Wei, A. M. Qin, G. G. Zhang, *International Journal of Electrochemical Science* 12(2017)5581.
 29. S. Li, M. Y. Wang, Y. Luo, J. G. Huang, *Acs Applied Mater Interfaces* 8(2016)17343.
 30. Q. H. Wu, R. F. Zhao, X. E. Zhang, W. L. Li, R. H. Xu, G. W. Diao, M. Chen, *Journal of Power Sources*, 359(2017)7.
 31. H. Liu, G. Wang, J. Park, J. Wang, H. Liu, C. Zhang, *Electrochim. Acta* 54(2009)1733.
 32. Y.N. NuLi, R. Zeng, P. Zhang, Z. P. Guo, H. K. Liu, *Journal of Power Sources* 184(2008)456.